# Nanoscale

Accepted Manuscript


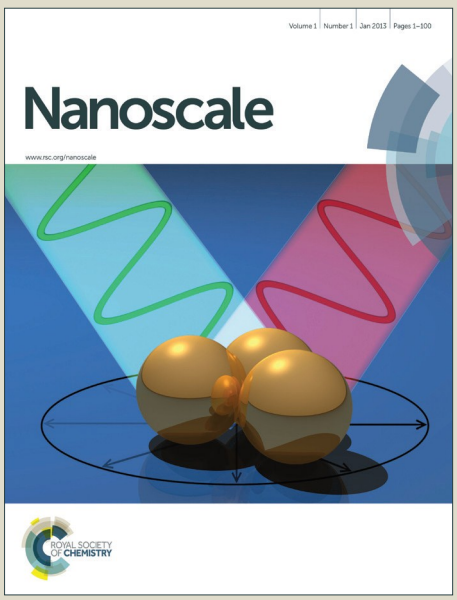





ROYAL SOCIETY OF CHEMISTRY

www.rsc.org/nanoscale

Journal Name

ARTICLE

# An inner filter effect based sensor of tetracycline hydrochloride as developed by loading photoluminescent carbon nanodots in the electrospun nanofibers

Received 00th January 20xx,
Accepted 00th January 20xx

DOI: 10.1039/x0xx00000x

www.rsc.org/

Min Lin[a], Hong Yan Zou[a], Tong Yang[a], Ze Xi Liu[a], Hui Liu[a*] and Cheng Zhi Huang[ab*]

Inner filter effect (IFE), which results from the absorption of the exciting or emission light by absorbers, has been employed as an alternative approach in sensing systems due to its flexibility and simplicity. In this work, highly photoluminescent carbon nanodots (CDs), which were simply prepared through a new one-step microwave synthesis route, were loaded in electrospun nanofibers, and the obtained nanofibers were then successfully applied to develop a fluorescent IFE-based visual sensor for tetracycline hydrochloride (Tc) sensing in milk. This developed visual sensor has high selectivity owing to the requiremts of the spectral overlap between the CDs and Tc, showing high promise in sensing chemitry with efficient response and economic effect.

## Introduction

During the past decades, numerous analytical techniques have been established based on fluorescence quenching (on-off) between fluorophores and specific targets,[1] and a new avenue for sensitive, selective, on-site detection of various targets has been opened up by different quenching mechanisms.[2] As a well-known phenomenon of fluorescence quenching, inner filter effect (IFE) results from the absorption of the exciting or emitted light by absorbers (namely, the quencher), wherein the absorption bands of the absorbers should possess a complementary overlap region with the excitation or emission band of the fluorophores. The degree of fluorescence quenching in IFE can be modulated by varying the absorbent concentrations, making the IFE-based process applicable in practice. [3-5] It is worth noting that an IFE system does not require any covalent linking between the fluorophore and the quencher. Therefore, it is obviously more simple and flexible than some common systems such as fluorescence resonance energy transfer (FRET), photoinduced electron transfer (PET) etc,[6, 7] wherein the donor and the acceptor are generally required to be kept in a particular distance and a complementary geometry besides the complementary overlap between the absorption bands of the absorbent species (acceptors) and the excitation or emission spectrum of the fluorophores (donors).

Owing to the inherent convenience, IFE has been widely employed in optical sensing chemistry over the past years.[8-11] For example, Xu et al employed the nanosized luminescent metal-organic framework to sensitively detect nitroaromatic explosives based on IFE.[11] Shang[12, 13] and Guo[14, 15] et al also developed a series of IFE-based analytical methods for detecting cyanide and cartap with AuNPs. It is also noticeable that noble metal nanopaticles and quantum dots (QDs) are the most universal nanostructures in these IFE-based sensing systems .[16] Recently, carbon nanodots (CDs) have gained tremendous attention as a rising star owing to the merits of easy-preparation, high-photochemical stability, low environmental impact, strong and tunable fluorescence emission properties,[17-19] and have shown high promise in analytical chemistry. [20-24]

Tetracyclines (TCs), a class of broad-spectrum and effective antibiotics, have been wide-spread distribution in pharmaceuticals, food and the environment.[25, 26] Conventional detections of TCs involve in high performance liquid chromatography (HPLC), capillary electrophoresis, GC/MS, etc.[27, 28] Most of these methods, however, require expensive instruments or present low sensitivity. Hence, it is of considerable importance to develop simple, low-cost, sensitive and rapid methods for TCs determination. Herein we developed a simple preparation method for fluorescent CDs through a facile microwave route by using citric acid (CA) as the carbon source and glutathione (GSH) as N,S source in the fashion of doping in order to improve the quantum yields of the carbon dots.[29-32] It was found that the fluorescence of the CDs could be easily quenched owing to the IFE of TCs. To make this IFE-based strategy for effective and practical applications, the as-prepared strong luminescent CDs are loaded into electrospun nanofibers which are known for having high surface area, good flexibility and cost-effective producibility.[33-35] Moveover, electrospun nanofibrous membranes (NFM) can provide a more

[a] Education Ministry Key Laboratory on Luminescence and Real-Time Analysis, College of Pharmaceutical Science, Southwest University, Chongqing 400715, China. E-mail: Chengzhi@swu.edu.cn, Tel:(+86) 23 68254659, Fax:(+86) 23 68367257.
[b] Chongqing Key Laboratory of Biomedical Analysis (Southwest University), Chongqing Science & Technology Commission, College of Chemistry and Chemical Engineering, Southwest University, Chongqing 400716,China.
Electronic Supplementary Information (ESI) available: Experimental section and additional figures (Fig. S1- S9). See DOI: 10.1039/x0xx00000x

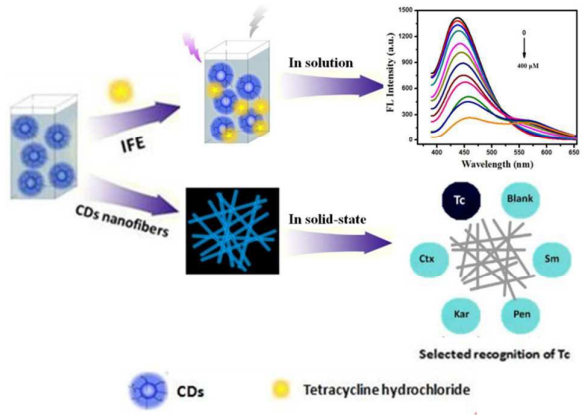


**Scheme 1** Illustration of the as-prepared CDs for Tc detection in solution and recognition in solid-state platform.

accessible and easier platform for sensing analytes. Poly (vinyl alcohol) (PVA) was chosen as a support matrix due to its electrospinnability, nontoxicity, and compatibility.[36] In order to protect the obtained nanofibers from dissolving in water, we prepare cross-linked CDs nanofibers similar to the reported literature,[36] for highly recognition of Tc in solid-state. Thus, this IFE-based technique might have broad, practical applications in the fields of drug analysis.

## 2. Experimental Section

### 2.1 Apparatus

All UV/Vis absorption and fluorescence spectra were obtained with UV-3600 and F-2500 spectrophotometer (Hitachi, Tokyo, Japan), respectively. A high resolution transmission electron microscope (Tecnai G2 F20 STWIN, FEI Company, USA) was used to characterize the morphology of the CDs. X-ray photoelectron spectra (XPS) of CDs was obtained with an ESCALAB 250 X-ray photoelectron spectrometer. X-ray powder diffraction (XRD) patterns were performed by a Shimadzu XRD-7000 (Beijing Purkinje General Instrument Co. Ltd) with Cu-Kα (1.5405 A) radiation source under the operating voltage and current of 40 kV and 50 mA. Fourier transform infrared spectroscopy (FTIR) of CDs was obtained with on a Shimadzu FTIR-8400S spectrometer (Kyoto, Japan). The Raman spectrum of the as-prepared CDs on Ag substrate was recorded with a Lab RAM HR800 Laser confocal Raman spectrometer (Horiba Jobin Yvon Inc., France) at ambient temperature (about 25 $^{o}$C). The fluorescence lifetime was measured with an FL-TCSPC fluorescence spectrophotometer (Horiba Jobin Yvon Inc., France). Fluorescence imaging was conducted on a DSU live-cell confocal microscope (Olympus, Japan) system with laser excitations of DAPI (CLSM). The morphologies and diameters of the as-prepared nanofibers were imaged by a Hitachi S-4800 scanning electron microscopy (SEM, Tokyo, Japan). A commercial DNF-001 electrospinning equipment (Beijing Kaiweixin Technology Co. Ltd., China) was employed for preparing CDs nanofibers.

### 2.2 Materials and regents

L-glutathione (GSH), citric acid (CA), tetracycline hydrochloride (Tc), cefotaxime, kanamycin, penicillin, streptomycin, procaine, nofloxiacin, ciprofloxacin, poly (vinyl alcohol) (PVA, 12 *wt* %, $M_w$ = 89, 000 ~ 98, 000) powder were purchased from Aladdin Chemistry Co. Ltd. (Shanghai, China). Quinine sulfate was obtained from Sigma-Aldrich. All other reagents were of analytical grade and used as received without further purification. All solutions were prepared with deionized water from a Millipore Milli-Q Ultrapure Water System.

### 2.3 Synthesis of CDs.

The fluorescent CDs were prepared through a simple, low-cost, one-step microwave synthesis route. Briefly, citric acid (0.42 g, 2 mmol) and glutathione (1.24 g, 4 mmol) were at first dissolved into 5 ml double distilled water, and then the solution was heated in a domestic microwave oven (maximum powder 750W, 2450MHz) for 5 min until the water in the mixture almost evaporated, during which the color of the mixture changed from light yellow to orange-yellow. The resultant solid was then dissolved in distilled water. After filtered by BIOSHARP membrane filters (0.22 μm), the resultant orange yellow and transparent aqueous solution was then subjected to dialysis ($M_w$ = 1000 Da) for 2 days to eliminate the overreacted residue.

### 2.4 Interaction of tetracycline hydrochloride (Tc) with CDs

Stock solution of Tc was first prepared with deionized water and then diluted into a series of concentrations. 0.1 mL of CDs solution (20 μg mL$^{-1}$) was mixed with 50 μL of Tc solution with various concentrations, then diluted to 1.0 mL with PBS buffer (pH 7.4) through mixing to form a homogeneous solution. The fluorescence emissions from 390 nm to 680 nm upon excitation of the light of 350 nm were measured after one minute.

### 2.5 A selective analysis of Tc in solid-state

The CDs/PVA NFM strips (1 cm × 1 cm） are immersed in different antibiotic solution (1mM) for one minute. Aftercontact and absorption of different solution, those strips are illuminated with a commercially 365 nm UV lamp to observe the color change with the naked eye.

### 2.6 Preparation of electrospun nanofibers loaded with CDs

Poly (vinyl alcohol) (PVA) (12 wt %, $M_w$ = 89, 000 ~ 98, 000), as a polymer host, was at first dissolved in 10 mL deionized water with vigorous stirring at 90 $^{o}$C for 3 h. 10 mg of CDs powder was then added to the PVA solution and stirred overnight at room temperature to obtain a brown and homogeneous CDs/PVA electrospun solution.

The CDs/PVA nanofibers were prepared by using a commercial DNF-001 electrospinning equipment under a high voltage of 25.0 kV by keeping the needle at a distance of 20 cm from the ground collector wrapped with aluminum foils. A syringe pump was applied to feed solutions to the needle at a rate of 1.8 mm/h.

In order to improve the water-stability of the CDs nanofibers, the as-prepared nanofibers were cross-linked through

glutaraldehyde (GA) vapour according to reference. [36] Briefly, the GA solution mixed with HCl in the volume ratio of 3:1 was at first spread out into a Petri dish, then the CDs nanofibrous membrane (NFM) and the GA-HCl dish were placed into a beaker sealing with preservative film under dehumidification system. The CDs NFMs were at last exposed to a GA vapor atmosphere for 24 h and kept in a vacuum oven to remove the remnant vapor molecules.

## 3. Results and discussion

### 3.1 Synthesis and characterization of CDs.

The CDs were prepared by a new developed facile microwave synthesis route, which can remarkably shorten the reaction time and improve the product purity. Dynamic monitoring of the product during the reaction was carried out (the details of these obtained CDs are seen in Fig S1-2 and Table S1, ESI†), which made the reaction mechanism involving the producing of CDs understanable. Considering the CDs prepared under 5 min has the best FL character (Table S1, ESI†) and a uniform size distribution, it is employed in the following experiments and dicussed in detail.

As Fig.1A shows, the as-prepared CDs are mono-dispersed and have an average size of 4.5 nm ranging from 3 to 7 nm, which is calculated by measuring the average size of 100 single CDs (Nano Measure Software). The high resolution TEM (HRTEM) image (inset of Fig. 1B) clearly shows that the as-prepared CDs have the lattice spacing of 0.21 nm and 0.31 nm, which may be attributed to the (100) facet of graphitic carbon and the spacing between graphene layers (002 facet), respectively.[37] The X-ray photoelectron spectroscopy (XPS) full survey spectrum of the obtained CDs, as shown in Fig.1C, presents four peaks at 163, 285, 400, and 532 eV, corresponding to S 2p, C 1s, N 1s and O 1s, respectively.[30, 38] This indicates that the CDs prepared from glutathione are doped with N and S. A high-resolution XPS spectrum of C1s

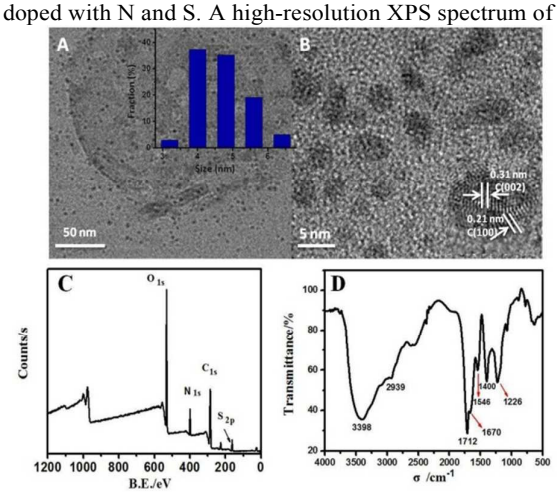


**Fig.1** Characterization of the as-prepared CDs. (A-B) HRTEM images and particles size distribution histograms of CDs; XPS (C) and FTIR spectra of the obtained CDs (D).

(Fig.S4A,ESI†) shows three dominant graphitic peaks at 284.6, 285.8 and 286.8 eV, corresponding to $sp^2$ C in graphene (C-C), $sp^3$ C in C-N, C-S C-O and C=O, respectively. It is noticeable that the peak at 288.4 eV, which is assigned to reported literatures, is not observed, indicating that –COOH groups is not present in the as-prepared CDs. [39, 40] The high-resolution N1s spectrum of the S, N-CDs (Fig.S4B, ESI†) shows three pronounced peaks at 399.3, 399.7 eV and 400.6 eV, which can be attributed to the pyrrolic N (C-N-C) and graphitic N or N-H bands, respectively. The S2p spectrum (Fig.S4C, ESI†) demonstrates that peaks at 163.9 and 162.9 eV are corresponding to the binding energy for the C-S-C units. FTIR spectrum (Fig.1D) exhibits characteristic absorption bands of O-H and N-H stretching vibrations at 3398 $cm^{-1}$, as evidenced by their vibrational fingerprints at 1546 $cm^{-1}$, C–N stretching vibrations at 1400 $cm^{-1}$. The peak at 1712 $cm^{-1}$ and 1670 $cm^{-1}$ indicate the existence of C=O, O=C-NH, similar to earlier reports. [41, 42] In a word, the as-prepared CDs are uniform with the size of about 4.5 nm, doped with N and S atoms, and both the XPS and FTIR measurements have showed that their surfaces are full of amide functional and hydroxyl groups, but short of carboxyl and thiol groups.

In order to understand the reaction mechanism involving the producing of CDs, a time course monitoring of the reaction was made at different reaction time intervals. With the increase of microwave irradiation time from 3 to 9 min, the color of the powders change from light yellow to brown (Fig. S2B), indicating that a varying degree of carbonization has occured. All the obtained CDs show high QYs which may result from similar functional groups on the surface (Fig.S2A). HRTEM images of these obtained CDs (Fig.S1) showed that it is hard to find obvious lattice fringes if the reaction time is relatively short such as 3 min, indicating that the degree of carbonization is insufficient. With reaction time increase, the average size of CDs gets decreased and distribution become narrow, the average size is 4.5 for 5 min and 2.7 nm for 9 min, for instance. However, with the reaction time further increase, to 20 min, for example, the size of particles obviously gets increasd with the distribution non-uniform, during which the color of powders change to dark brown, indicating excessive carbonization. Thus, a possible mechanism for the formation of CDs with the efficient heating by the microwave-assisted treatment for a homogeneous precursors might be the dehydration, condensation, polymerization, and thermal carbonization, which lead to for formaiotn of nucleation, and then the nuclei get grown by the diffusion of solutes towards the particle surface.[35, 43]

### 3.2 Optical properties of the obtained CDs.

The UV-vis absorption spectrum (Fig. 2A) shows that the as-prepared CDs have two characteristic absorption peaks at 248 and 344 nm, respectively. The strong absorption at 248 nm owes to a large amount of π-electrons in the $sp^2$ hybridised islands, while that at 344 nm is mainly attributed to the n- π* transition of the C=O and C=N bonds. Under the irradiation of 365 nm UV light lamp, the CDs aqueous solution present bright blue color (Fig. 2A inset) and the maximum FL emission is

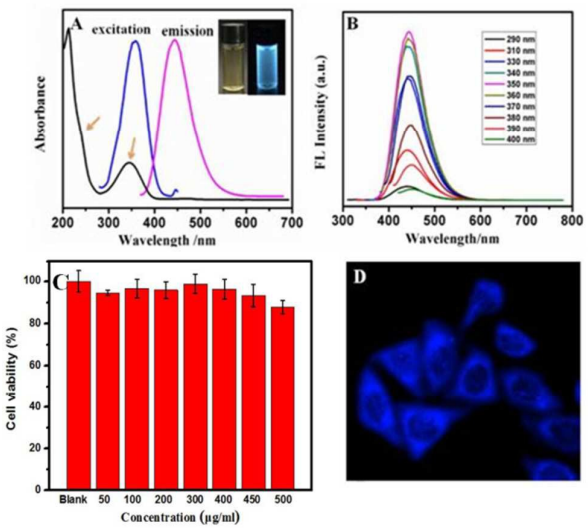


**Fig.2** Optical and bioactive properties of the as-prepared CDs. (A) UV absorption and FL spectra of CDs. UV-Vis spectra (black line), excitation fluorescence spectrum (blue line) and fluorescence emission (pink line); the inset optical images under (left) daylight and (right) UV light. (B) FL emission spectra of CDs under different excitation wavelengths from 290 to 400 nm. (C) Cellular toxicity of CDs on Hep-2 cell viability; (D) Cellular images by excitation at DAPI channel (350 -360 nm).

located at 445 nm when excited at 350 nm. A notable phenomenon is that the emission at 445 nm is excitation wavelength independent (EIE) with the excited light beam from 290 to 400 nm (Fig. 2B), indicating that the CDs process a uniform distribution of the surface state. The quantum yield (QY) of the as-prepared CDs is 46.9% by calibrating against reference quinine sulfate in 0.1 M $H_2SO_4$ (Fig.S5, ESI†). The comparatively high QY value might be attributed to the radiative recombination of electron-hole pairs trapped on the surface defect of CDs, which can remain active in the presence of N, S-atoms, just as previous literatures demonstrated. [44] The as-prepared CDs are very stable in salt solution even if the concentrations of NaCl is as high as 0.5 M (Fig.S6A, ESI†) and also photostable even illuminated under the light of 150 w Xe lamp for 1h (Fig.S6B, ESI†). The CKK-8 assay assessment showed that the cytotoxicity of CDs is very low (Fig. 2C), and the viability of Hep-2 cells remained greater than 90% even if incubated with an relatively high concentrations ( 400 μg $mL^{-1}$ ) for 24h. Furthermore, most of the CDs get into the cytoplasmic area as observed from DAPI channel (Fig. 2D), suggesting that the as-prepared CDs can be used for cytoplasmic staining, labelling and targeting. Above results indicate that the as-prepared CDs present excellent optical properties and have the potential of promising fluorescent nanoprobe.

### 3.3 IFE bewteen CDs and Tc.

It was found that the excellent fluorescent properties of CDs could be selectively quenched by Tc (Fig.S7A, ESI†), revealing the possibility of applying the as-prepared CDs as a sensitive fluorescent chemosensor of Tc (Fig.S8A-B, ESI†).

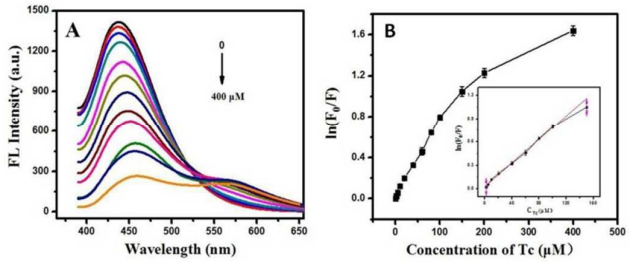


**Fig.3** The sensitivity of CDs for Tc detection. (A) Fluorescence responses of CDs upon various concentrations of Tc (from top to bottom, 0, 2, 5, 10, 20, 40, 60, 80, 100, 150, 200 and 400 μM) in pH 7.4 PBS solution. (B) The linear relationship between $F_0/F$ and Tc concentration (CDs, 2μg $mL^{-1}$, excitation wavelength, 350 nm)

The fluorescence quenching can be described by Stern−Volmer's equation: [45]

$$\frac{F_0}{F} = 1 + K_{SV}c_q = 1 + K_q\tau_0 c_q \qquad (1)$$

where $F_0$ and $F$ are the fluorescence intensities of the fluorophores in the absence and in the presence of a quencher respectively; $c_q$ is the concentration of the quencher, $K_{SV}$ is the dynamic quenching constant, and in this case $K_{sv}$ = 0.0112 $\mu M^{-1}$ by taking the slope of the regression line in Fig.3B. $K_q$ is the quenching rate constant and $\tau_0$ is the fluorescence lifetime of CDs ($\tau_0$ = 11.06 ns). $F_0/F$ displays the good linear relationship with Stern-Volmer plot. The resulted $K_q$ has the value of $0.995 \times 10^{12}$ $M^{-1}$ $s^{-1}$ , suggesting a static quenching rather than a dynamic quenching in accordance that the rate constant of a dynamic quenching is usually less than $1.0\times 10^{10}$ $M^{-1}$ $s^{-1}$.[45, 46] Furthermore, The linear range for Tc is $2 \times 10^{-6}$ to $1.5\times10^{-4}$ mol $L^{-1}$ with a limit of detection of $5.2\times10^{-7}$ mol $L^{-1}$ (Fig.3B), which is comparable to other previously reported values.[47]

To further explore the sensing mechanism, a series of studies are carried out. There is a good spectral overlap between the absorption band of the Tc and the excitation or emission band of the CDs (Fig. 4A), suggesting that the fluorescence quenching might be related to FRET, IFE process, and even if electron transfer mechanisms. Since the lifetime of the CDs both in the absence and prescence of Tc remain unchanged (Fig. 4B), thus fluorescence quenching is unresonable ascribed to FRET process. Then, the lowest unoccupied molecular orbital energy levels ($E_{LUMO}$) and the highest occupied molecular orbital ($E_{HUMO}$) of CDs (Fig. 4C) are estimated as – 3.91 eV and -7.01 eV according to the empirical formula (Fig. S9, ESI†).[29] Meanwhile, the $E_{HOMO}$ and $E_{LUMO}$ of Tc could be calculated as -3.87 eV and -6.2 eV, respectively by B3LYP method in Dmol3 mode. Obviously, as shown in Fig.4C, photo-excited electrons in CDs are not energetically allowed to undergo electron transfer from LUMO of the CDs to LUMO of the Tc, which also excludes electron transfer mechanism between CDs and Tc. Therefore, the IFE might be considered as one major process in the fluorescence quenching.

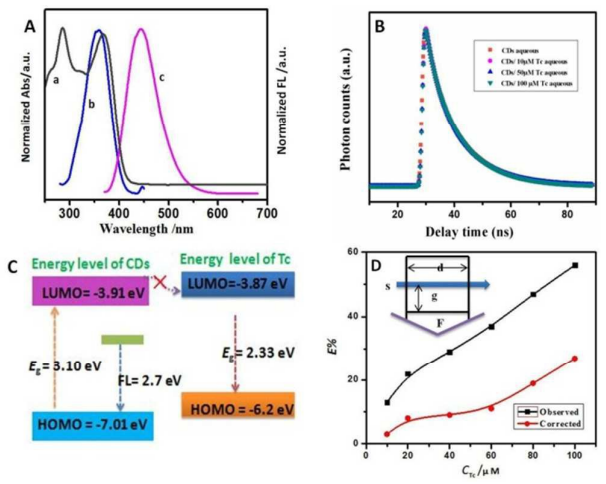


**Fig.4** The mechanism of Tc quenching fluorescence of CDs. (A)UV-vis absorption spectrum of Tc (a) and fluorescence excitation (b) and emission (c) spectra of CDs; (B) The time-correlated single-photon counting (TCSPC) of CDs alone and CDs with different concentrations of Tc (10 μM, 50 μM, 100 μM); (C) The LUMO and HOMO of CDs and Tc; (D) Suppressed efficiency ($E$%) of observed (black curve) and corrected (red curve) measurements for CDs after each addition of different concentrations of Tc, $E= 1 - F/F_0$. $F_0$ and $F$ are the steady-state fluorescence intensities of CDs in the absence and presence of Tc, respectively.

**Table 1.** IFE of Tc on the fluorescence of CDs

| Tc (μM) | $A_{ex}$ | $A_{em}$ | $CF$ | $F_{obsd}$ | $F_{cor}$ | $F_{corr,0}/F_{corr}$ |
|---|---|---|---|---|---|---|
| 0 | 0.08 | 0.001 | 1.10 | 1421 | 1553.2 | 1 |
| 10 | 0.182 | 0.001 | 1.23 | 1230 | 1512.9 | 1.03 |
| 20 | 0.227 | 0.001 | 1.28 | 1120 | 1433.6 | 1.08 |
| 40 | 0.316 | 0.002 | 1.41 | 1009 | 1422.7 | 1.10 |
| 60 | 0.42 | 0.002 | 1.56 | 891 | 1390 | 1.12 |
| 80 | 0.493 | 0.002 | 1.67 | 755 | 1260.9 | 1.23 |
| 100 | 0.575 | 0.002 | 1.80 | 626 | 1126.8 | 1.38 |

$A_{ex}$ and $A_{em}$ are the absorbance of Tc with the addition of CDs at 350 nm and 445 nm, respectively. Corrected factor (CF) is calculated as $F_{cor}/F_{obsd}$. $F_{obsd}$ is the measured fluorescence intensity of CDs with the addition of Tc at 445 nm. $F_{cor}$ is the corrected fluorescence intensity with eq 1 by removing IFE from the measured fluorescence intenstity. $F_{cor,0}$ and $F_{cor}$ are the corrected fluorescence intensities of CDs in the absence and presence of Tc, respectively.

Furthermore, the selectivity toward Tc could also be explained by the IFE mechanism (Fig.S57, ESI†). Tc has higher molar extinction efficient ($\varepsilon$= 5520) at 350 nm in accordance with the excitation wavelength of CDs than other antibiotics (Fig.S7B, Table S3, ESI†) which resulted in high IFE efficiency. Since IFE can be estimated according to eq 1. [22, 46, 48]

$$\frac{F_{corr}}{F_{obsd}} = \frac{2.3dA_{ex}}{1-10^{-dA_{ex}}} \cdot \frac{sA_{em}10^{gA_{em}}}{1-10^{-sA_{em}}} \qquad (2)$$

Wherein, $F_{obsd}$ is the measured maximum fluorescence intensity and $F_{cor}$ is the corrected fluorescence intensity by removing IFE from the measured fluorescence intensity $F_{obsd}$; $A_{ex}$ and $A_{em}$ are the absorbance of CDs with the addition of Tc at 350 nm and 445 nm, respectively; $g$ is the distance between the edge of the excitation beam and the edge of the cuvette (0.40 cm in this case), while $s$ is the thickness of excitation beam (0.10 cm), and $d$ is the width of the cuvette (1.00 cm). The correction factor (CF) of IFE ($F_{cor}/F_{obsd}$) at each concentration of Tc thus could be calculated (Table 1) . After the IFE was removed from the totally observed suppressed fluorescence, the suppressed efficiency for the totally observed and the corrected fluorescence of Tc is figured out, as shown in Fig.4D, We find that approximately half of the qunench effect come from the IFE of Tc, which shows some other quenching mechanism coexisting.

In addition, the FTIR spectrum of the CDs- Tc system shows the vibrations of C-OH is red shifted by 27 $cm^{-1}$ with respect to that of the initial CDs (from 3371 to 3398 $cm^{-1}$) (Fig.S10, ESI† ),[41] suggesting the formation of hydrogen bonding, which indicated the fluorescence quenching may partly attribute to molecular interactions.[45]

### 3.4 A fluorescent IFE-based visual sensor in solid-state.

Considering that solid-state sensor could supply a feasible and superior platform to maintain their stability and rapidly for detecting analytes, and electrospinning, which is characterized by large surface area to volume ratio, high porosity and excellent mechanical properties,[33, 36] has been recognized as one of the easiest and superior approaches to prepare electrospun nanofibrous sensors. Herein we thus develop a visual, solid-state sensor for highly selective recognition of Tc based on coupling CDs and electrospun nanofibers.

It is known that the obtained nanofibrous membrane (NFM) are very easy to solve in water when PVA is employed as a

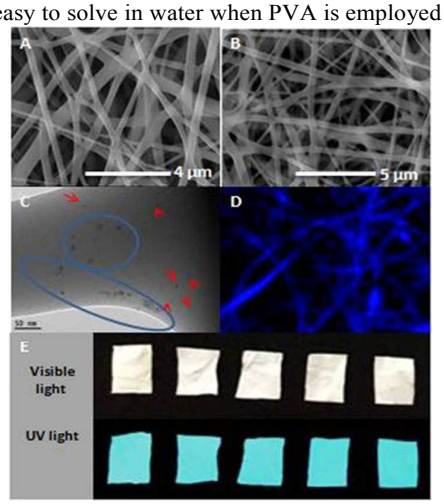


**Fig.5** Characterization of the obtained CDs/PVA nanifibrous membrane (NFM). (A-B) SEM images of CDs/PVA nanofibers after crosslinking; (C) TEM image of the CDs loaded into PVA nanofibers; (D) CLSM image of the CDs/PVA NFM excited at DAPI channel. (E) Photographs of the CDs/PVA strip (2 cm × 2 cm ) viewed under UV and visiblelight.

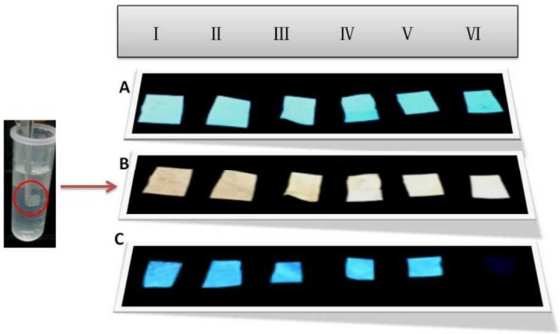


**Fig. 6** Visual sensing of tetracycline. Photographs of the PVA NFM strips ( 1 cm × 1 cm ) before different antibiotics treatment (1 mM) under UV (A) and white light (B); Fluorescence response under UV light towards different antibiotics solution(C) (from left to right): (I) water (control); (II) cefotaxime; (III) kanamycin; (IV) penicillin; (V) streptomycin and (VI ) tetracycline.

matrix (Fig.S11A. ESI†). Hence, the CDs/PVA NFM are further cross-linked with glutaraldehyde vapor, which can be seen that the nanofibers become very flexible in water and are suitable for further study (Fig.S13B. ESI†). Thus, all the rest of the characterizations are performed after cross-linking. Fig.5A-B depict the SEM images of the as-fabricated nanofibers, which exhibit a beadless, defect-free morphology with a relatively uniform diameter of 390 ± 84 nm (Fig.S12, ESI†), suggesting the PVA ratio (12 wt %) is appropriate and have a good electrospinnability. As shown in Fig.5C, these small CDs have been indeed loaded in the PVA nanofibers, though they are not very easy to be observed which may result from the thick copper mesh in characterization. Further confirmed by the CLSM images (Fig.5D), the observed blue fluorescence is the characteristic emission of CDs, indicating the homogeneous distribution of CDs in the nanofibers. Moreover,on exposure to UV light (365 nm), the CDs/PVA NFM strips (2 cm × 2 cm) emit bright blue fluorescence which confirm this approach could retain the original fluorescence efficiency of CDs (Fig.5E). All the observed results indicate the obtained CDs/PVA nanofibers are favorable as a solid-state sensing platform for analytes.

As depicted in Fig.6, the sensing performance of CDs/PVA nanofibers towards various antibiotics in an aqueous solution has been tested. Before immersing in the solution (Fig.6A-B), all the NFM strips (1 cm × 1 cm） emit strong and comparable blue flourescence. As shown in Fig.6C, after contact and absorption of different solution respectively, significant darkening can only be observed in the one strip which has absorbed Tc under a commercially 365 nm UV lamp with the naked eye. Other strips retain their original blue color.

### 3.5 Determination of Tc in milk

For investigating the applicability of the developed sensor in facing up real complicate samples, the visual sensing was made for the recognition of Tc in milk. With general elementary treatments widely adopted in milk analysis by removing protein, fat and other organic substances during the sample preparation procedure,[49]

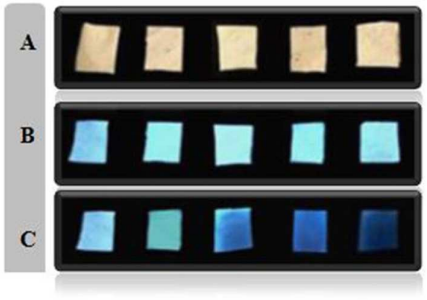


**Fig.7** Validation of the proposed method in milk samples. Photographs of the PVA NFM strips ( 1 cm × 1 cm ) in the daylight (A) and under 365 nm UV light (B); (C) Photographs of the PVA NFM strips after soaking in real sample solution containing different concentrations (from left to right: 0, 12, 40, 75, 100 μM ) under 365 UV light.

quantities of Tc as added into milk could be very easily visually observed since the blue fluorescence of the NFM strips was immediately quenched under a commercially 365 nm UV lamp (Fig. 7). This unique and exclusive fluorescence quenching phenomenon towards Tc indicates that the solid-state nanofibrous sensor has the ability to recognize Tc in the fileds of food control or drug analysis with rapid response and economic effect.

## Conclusions

In summary, highly photoluminescent carbon nanodots (CDs), which could be qualified as a stable fluorescent probe, are prepared through a facile microwave-assisted method. The fluorescence of the as prepared CDs could be intensively quenched by tetracycline hydrochloride (Tc) owing to the inner filter effect (IFE), and thus a visual sensor for Tc in milk samples was developed with the IFE, which is more efficient and convenient than most reported solution-based techniques. In brief, this IFE-based exploration will pave a new way for the determination of Tc in real-world.

## Acknowledgements

All authors thank the financial supports from the National Natural Science Foundation of China (NSFC, 21535006) and Chongqing Graduate Student Scientific Research Innovation Project (CYS, 2015056).

## Notes and references

1. J. Wu, W. Liu, J. Ge, H. Zhang and P. Wang, *Chem. Soc. Rev.*, 2011, **40**, 3483-3495.

2. H. X. Zhao, L. Q. Liu, Z. D. Liu, Y. Wang, X. J. Zhao and C. Z. Huang, *Chem. Commun*, 2011, **47**, 2604-2606.

3. S. Yang, C. Wang, C. Liu, Y. Wang, Y. Xiao, J. Li, Y. Li and R. Yang, *Anal. Chem.*, 2014, **86**, 7931-7938.

4. N. Shao, Y. Zhang, S. Cheung, R. Yang, W. Chan, T. Mo, K. Li and F. Liu, *Anal. Chem.*, 2005, **77**, 7294-7303.

5. L. Wang, J. Zheng, Y. Li, S. Yang, C. Liu, Y. Xiao, J. Li, Z. Cao and R. Yang, *Anal.Chem*, 2014, **86**, 12348-12354.

6. W. Wei, C. Xu, J. Ren, B. Xu and X. Qu, *Chem. Commun.*, 2012, **48**, 1284-1286.

7. H. Zhang, Y. Chen, M. Liang, L. Xu, S. Qi, H. Chen and X. Chen, *Anal.Chem*, 2014, **86**, 9846-9852.

8. H. Kim, B. I. Lee and S. H. Byeon, *Chem.Commun.*, 2015, **51**, 725-728.

9. Y. Zhai, L. Jin, P. Wang and S. Dong, *Chem. Commun.*, 2011, **47**, 8268-8270.

10. S. Huang, F. Zhu, Q. Xiao, W. Su, J. Sheng, C. Huang and B. Hu, *RSC Adv.*, 2014, **4**, 46751-46761.

11. H. Xu, F. Liu, Y. Cui, B. Chen and G. Qian, *Chem. Commun*, 2011, **47**, 3153-3155.

12. L. Shang, C. Qin, L. Jin, L. Wang and S. Dong, *The Analyst*, 2009, **134**, 1477-1482.

13. L. Shang and S. Dong, *Anal. Chem.*, 2009, **81**, 1465-1470.

14. J. Guo, X. Liu, H. Gao, J. Bie, Y. Zhang, B. Liu and C. Sun, *RSC Adv.*, 2014, **4**, 27228-27235.

15. J. Guo, Y. Luo, H. Li, X. Liu, J. Bie, M. Zhang, X. Cao, F. Shen, C. Sun and J. Liu, *Anal. Methods.*, 2013, **5**, 6830-6838.

16. H. Han, V. Valle and M. M. Maye, *J.Phys.chem.C*, 2012, **116**, 22996-23003.

17. S. Y. Lim, W. Shen and Z. Gao, *Chem Soc Rev*, 2015, **44**, 362-381.

18. P. G. Luo, S. Sahu, S.-T. Yang, S. K. Sonkar, J. Wang, H. Wang, G. E. LeCroy, L. Cao and Y.-P. Sun, *J Mater Chem B*, 2013, **1**, 2116.

19. Y. F. Kang, Y. H. Li, Y. W. Fang, Y. Xu, X. M. Wei and X. B. Yin, *Scientific reports*, 2015, **5**, 11835.

20. Y. Dong, R. Wang, G. Li, C. Chen, Y. Chi and G. Chen, *Anal. Chem.*, 2012, **84**, 6220-6224.

21. M. Zheng, Z. Xie, D. Qu, D. Li, P. Du, X. Jing and Z. Sun, *ACS Appl. Mater. Interfaces.*, 2013, **5**, 13242-13247.

22. X. Zhu, T. Zhao, Z. Nie, Y. Liu and S. Yao, *Anal. Chem.*, 2015, **87**, 8524-8530.

23. S. Mandani, B. Sharma, D. Dey and T. K. Sarma, *Nanoscale*, 2015, **7**, 1802-1808.

24. X. Gao, Y. Lu, R. Zhang, S. He, J. Ju, M. Liu, L. Li and W. Chen, *J.Mater.Chem.C*, 2015, **3**, 2302-2309.

25. J. M. Traviesa-Alvarez, J. M. Costa-Fernández, R. Pereiro and A. Sanz-Medel, *Anal. Chim.Acta*, 2007, **589**, 51-58.

26. H. Tan and Y. Chen, *Sens. Actuators B: Chem*, 2012, **173**, 262-267.

27. G. T. Peres, S. Rath and F. G. R. Reyes, *Food Control*, 2010, **21**, 620-625.

28. T.-Y. Ma, T. W. Vickroy, J.-H. Shien and C.-C. Chou, *Electrophoresis*, 2012, **33**, 1679-1682.

29. Y. Guo, Z. Wang, H. Shao and X. Jiang, *Carbon*, 2013, **52**, 583-589.

30. Z. L. Wu, M. X. Gao, T. T. Wang, X. Y. Wan, L. L. Zheng and C. Z. Huang, *Nanoscale*, 2014, **6**, 3868-3874.

31. D. Qu, M. Zheng, P. Du, Y. Zhou, L. Zhang, D. Li, H. Tan, Z. Zhao, Z. Xie and Z. Sun, *Nanoscale*, 2013, **5**, 12272-12277.

32. Y. Xu, M. Wu, Y. Liu, X. Z. Feng, X. B. Yin, X. W. He and Y. K. Zhang, *Chem-Eur. J* 2013, **19**, 2276-2283.

33. T. Yang, H. Yang, S. J. Zhen and C. Z. Huang, *ACS Appl. Mater. Interfaces*, 2015, **7**, 1586-1594.

34. X. Sun, Y. Liu, G. Shaw, A. Carrier, S. Dey, J. Zhao and Y. Lei, *ACS Appl Mater Interfaces*, 2015, **7**, 13189-13197.

35. X. Zhai, P. Zhang, C. Liu, T. Bai, W. Li, L. Dai and W. Liu, *Chem Commun*, 2012, **48**, 7955-7957.

36. A. Senthamizhan, A. Celebioglu and T. Uyar, *J. Mater. Chem. A*, 2014, **2**, 12717-12723.

37. E. Ju, Z. Liu, Y. Du, Y. Tao, J. Ren and X. Qu, *ACS Nano*, 2014, **8**, 6014-6023.

38. Z. L. Wu, P. Zhang, M. X. Gao, C. F. Liu, W. Wang, F. Leng and C. Z. Huang, *J Mater Chem B*, 2013, **1**, 2868.

39. D. Qu, M. Zheng, L. Zhang, H. Zhao, Z. Xie, X. Jing, R. E. Haddad, H. Fan and Z. Sun, *Sci.Rep.*, 2014, **4**, 5294.

40. D. Qu, Z. Sun, M. Zheng, J. Li, Y. Zhang, G. Zhang, H. Zhao, X. Liu and Z. Xie, *Adv Opt Mater*, 2015, **3**, 360-367.

41. M. Yang, H. Li, J. Liu, W. Kong, S. Zhao, C. Li, H. Huang, Y. Liu and Z. Kang, *J .Mater .Chem. B*, 2014, **2**, 7964-7970.

42. J. Ju and W. Chen, *Biosensors & bioelectronics*, 2014, **58**, 219-225.

43. H. Huang, C. Li, S. Zhu, H. Wang, C. Chen, Z. Wang, T. Bai, Z. Shi and S. Feng, *Langmuir*, 2014, **30**, 13542-13548.

44. Y. Dong, H. Pang, H. B. Yang, C. Guo, J. Shao, Y. Chi, C. M. Li and T. Yu, *Angewandte Chemie*, 2013, **52**, 7800-7804.

45. J. R. Lakowicz, *Principles of Fluorescence Spectroscopy, 2 nd ed*, New York, 1999, .

46. W. Zhai, C. Wang, P. Yu, Y. Wang and L. Mao, *Anal. Chem.*, 2014, **86**, 12206-12213.

47. J. Hou, J. Yan, Q. Zhao, Y. Li, H. Ding and L. Ding, *Nanoscale*, 2013, **5**, 9558-9561.

48. T. D. Gauthier, E. C. Shane, W. F. Guerin, W. R. Seitz and C. L. Grant, *Environ. Sci . Technol*, 1986, **20**, 1162-1166.

49. M. Ramezani, N. Mohammad Danesh, P. Lavaee, K. Abnous and S. Mohammad Taghdisi, *Biosens Bioelectron*, 2015, **70**, 181-187.